Work-Function Engineering of Graphene Electrodes by Self-Assembled Monolayers for High-Performance Organic Field-Effect Transistors

Jaesung Park,[†,⊥] Wi Hyoung Lee,[‡,⊥] Sung Huh,[†] Sung Hyun Sim,[§,‖] Seung Bin Kim,[†] Kilwon Cho,*[‡] Byung Hee Hong,*[§,‖] and Kwang S. Kim*[†]

[†]Center for Superfunctional Materials, Department of Chemistry and [‡]Department of Chemical Engineering, Pohang University of Science and Technology, Pohang 790-784, Korea

[§]SKKU Advanced Institute of Nanotechnology (SAINT) and Center for Human Interface Nano Technology (HINT) and [‖]Department of Chemistry, Sungkyunkwan University, Suwon 440-746, Korea

Ⓢ Supporting Information

ABSTRACT: We have devised a method to optimize the performance of organic field-effect transistors (OFETs) by controlling the work functions of graphene electrodes by functionalizing the surface of SiO_2 substrates with self-assembled monolayers (SAMs). The electron-donating NH_2-terminated SAMs induce strong n-doping in graphene, whereas the CH_3-terminated SAMs neutralize the p-doping induced by SiO_2 substrates, resulting in considerable changes in the work functions of graphene electrodes. This approach was successfully utilized to optimize electrical properties of graphene field-effect transistors and organic electronic devices using graphene electrodes. Considering the patternability and robustness of SAMs, this method would find numerous applications in graphene-based organic electronics and optoelectronic devices such as organic light-emitting diodes and organic photovoltaic devices.

SECTION: Electron Transport, Optical and Electronic Devices, Hard Matter
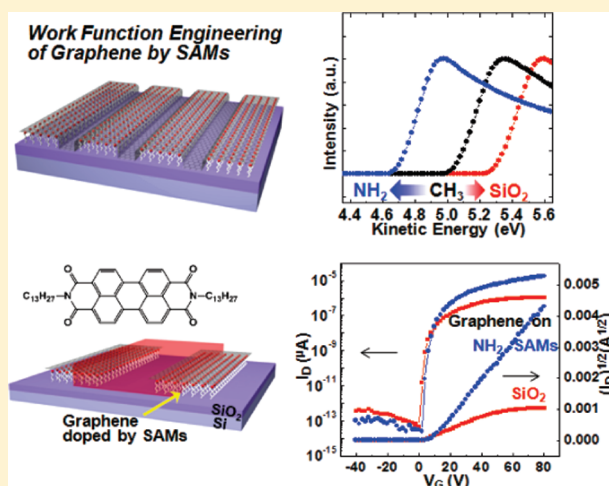
There has been much interest in doping of graphene because tunable electrical properties of graphene are attainable by instantaneous doping.[1−6] For example, depositing the dopant atoms on graphene surface induces interstitial doping by charge transfer process between graphene and dopant atoms, which results in change in work function of graphene.[1,7,8] However, H_2O (p-type) or NH_3 (n-type) molecules in the atmosphere can also dope graphene,[2,9] which makes it difficult to control the position and magnitude of doping. For this reason, interstitial doping investigated so far is usually done under vacuum condition to avoid unwanted adsorption of dopant molecules. To this end, a new type of doping method needs to be developed to finely tune the electrical properties of the graphene-based electronic devices.

Self-assembled monolayers (SAMs) have been receiving considerable attention as an ultrathin layer can be uniformly constructed on oxide surface by self-assembly method.[10] The fabrication process of SAMs is simple. The robust ultrathin layer in a defined area is constructed by spontaneous chemical reaction at the interface, which makes SAMs technologically attractive for surface and interface engineering. In addition, surface energy, dipole moment and chemical reactivity of surface can be easily tuned by attaching functional groups in SAMs.[11] These functions allow SAMs to be used as a buffer layer in nanoscale optoelectronic devices.[10,12] Thus, there should be possibility for the use of SAMs as a buffer layer to induce instantaneous doping of graphene and tune the work function of graphene.

We report here the use of SAMs to control the work functions of graphene electrodes for high-performance OFETs. The doping types and position are determined by patterning SAMs with different functional groups. The effects of doping on the electrical properties of graphene are investigated using graphene as an active channel layer or electrode material. It is important to note that graphene doped by SAMs displays a Dirac voltage shift over 150 V in transistor application and enables graphene to have a tunable work function of 3.9 to 4.5 eV. These factors impact the
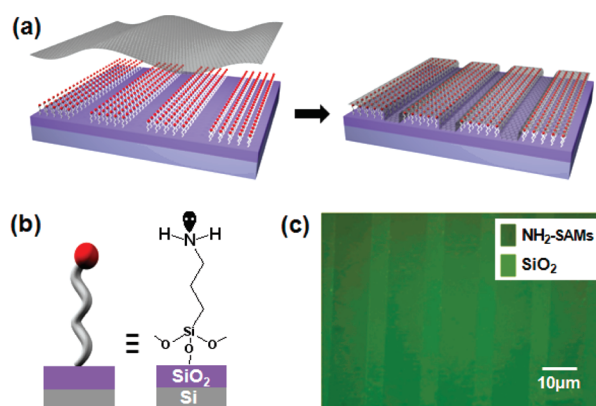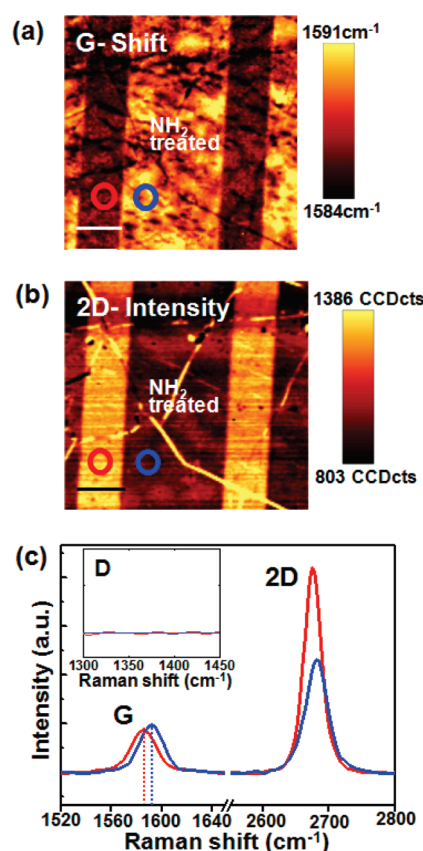
Figure 1. (a) Schematic transfer process of monolayer graphene on patterned self-assembled monolayer (SAM)-modified SiO$_2$ substrate. (b) Molecular structure of amine (NH$_2$)-functionalized SAMs on SiO$_2$/Si substrate. (c) Optical microscope image of patterned NH$_2$-SAMs on SiO$_2$/Si substrate.


Figure 2. Raman spectra of monolayer graphene on SiO$_2$/Si substrate with patterned NH$_2$-SAMs. (a) Raman maps of the G-bands shift. (b) Raman maps of the 2D bands (2620–2740 cm^{-1}) intensity. Scale bars are 10 μm. (c) Raman spectra from the marked spots with corresponding colored circles. Inset shows magnified spectra of the D-bands (1300–1450 cm^{-1}).

electrical properties of organic electronic device using graphene electrodes.

Monolayer graphene was synthesized utilizing the CVD process described in the literature.[13−15] The graphene film grown on the copper foil was covered by polymethylmethacrylate (PMMA) and floated in an aqueous solution of 0.1 M ammonium persulphate ((NH_2)$_4$S$_2$O$_8$). After all the copper layers were etched away, the graphene film with PMMA support was transferred to the SAMs-modified SiO$_2$ substrate. The detailed fabrication procedure of SAMs and the characteristics are in the Supporting Information.

Figure 1a shows a schematic illustration of the transfer process of graphene onto the SAM-modified SiO$_2$ substrate. Graphene on SAMs can be doped by the charge transfer process between functional group in SAMs and graphene. For instance, SAMs with an amine (NH$_2$−) functional group (aminotriethoxysilane) have lone pair electrons, and these groups exhibit electron-donating characteristics (Figure 1b).[16] For this reason, graphene is n-doped when a graphene film is in contact with the NH$_2$-functional group in SAMs. An exciting merit of doping using SAMs is its patternability. SAMs can be patterned in a defined area by utilizing patterned photoresist as blocking layer for SAMs deposition. (See the Supporting Information for the fabrication procedure.) Figure 1c shows patterned NH$_2$−SAMs with line width of 10 μm.

To analyze the selective area doping behavior of graphene on patterned SAMs, we obtained Raman maps of the G and 2D bands, which are shown in Figure 2a,b. It is clear that the Raman map of the G-band shift exhibits a bright colored region at the NH$_2$−SAMs patterned area. In contrast, the Raman map of 2D band intensity shows the opposite trend. The Raman spectra for the area marked with blue circles (NH$_2$−SAMs modified area) show a blue shift of the G band (from 1585 to 1594 cm^{-1}) and a decrease in 2D band intensity (Figure 2c). These changes in peak position and intensity demonstrate that graphene is effectively doped by SAMs.[3,17] Furthermore, the intensity ratio of 2D-band/G-band and full width at half-maximum (fwhm) of the 2D band supports selective area doping of graphene by SAMs (Supporting Information, Figure S1).[4,17] Because there is no discernible D peak in graphene films on SiO$_2$ or NH$_2$−SAM-modified SiO$_2$, defects are not associated with the doping process. For this

reason, the doping process in this approach is different compared with destructive doping techniques of graphene such as substitutional doping of graphene or covalent functionalization of graphene, as previously reported.[18] Because the G peak is known to increase for both electron and hole doping,[3,4] it is necessary to define the type of doping using other spectroscopic analyses.

Figure 3a shows ultraviolet photoemission spectra (at the secondary electron emission region) of graphene films on different SAMs. Because the onset of the secondary electrons corresponds to the vacuum level of the graphene relative to the Fermi level, the doping type and degree can be derived by calculating the work function (Φ) of graphene from the equation[19]

$$\phi = \hbar\omega - |E_{\text{sec}} - E_{\text{FE}}| \qquad (1)$$

where $\hbar\omega$ = 21.2 eV (He I Source), E_{sec} is the onset of the secondary emission, and E_{FE} is the Fermi edge (22.0 eV from the valence band spectrum (sample bias at −5 V) in the 4B1 beamline at Pohang Accelerator Laboratory). The work functions of graphene on NH$_2$−SAM-and CH$_3$−SAM (octadecyltrichlorosilane)-modified SiO$_2$s and untreated SiO$_2$ were obtained to be 3.9, 4.25, and 4.5 eV, respectively. In a previous report, the work function of CVD-grown monolayer graphene on a noninteracting polymer substrate was ∼4.3 eV.[14] This value corresponds to the work function of graphene on the

842

dx.doi.org/10.1021/jz200265w |*J. Phys. Chem. Lett.* 2011, 2, 841–845
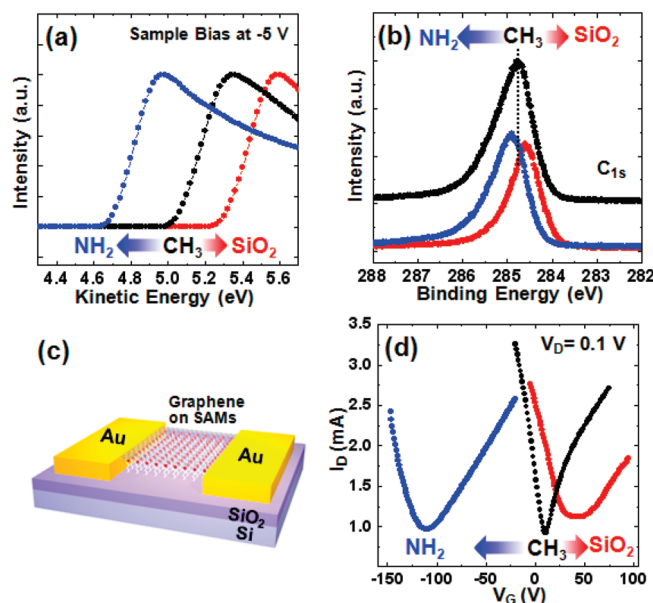
Figure 3. (a) Ultraviolet photoemission spectra (at the secondary electron emission region) of the graphene films on different SAM-modified SiO_2/Si substrates. (b) XPS carbon 1s peaks (C_{1s}) of the graphene films on different SAM-modified SiO_2/Si substrates. (c) Schematic of the graphene field-effect transistors (FETs) having SAMs as an insertion layer. (d) Current−voltage transfer characteristics of the graphene FETs on different SAM-modified SiO_2/Si substrates. CH_3: octadecyltrichlorosilane; NH_2: aminotriethoxysilane; SiO_2: untreated; V_D: drain voltage; V_G: gate voltage; I_D: drain current.

CH_3−SAM-modified SiO_2 substrate (4.25 eV). Because no interaction exists between graphene and the CH_3 groups in SAMs, the graphene on CH_3−SAM-modified SiO_2 may have little tendency toward substrate-induced doping. However, external doping from impurities can be incorporated into the graphene film during the synthesis and transfer process. The work function of graphene on the SiO_2 substrate increases by 0.25 eV, compared with the CH_3−SAM-modified SiO_2 substrate. This implies that extra holes are incorporated into graphene (p-doping) and thus lowers the Fermi level from the Dirac point.[20,21] On the NH_2−SAM-modified SiO_2 substrate, we see the work function decrease by 0.35 eV. It seems that the lone-pair electrons in NH_2−SAMs induce extra electrons in graphene, which raises the Fermi level from the Dirac point (n-doping). These doping behaviors depend on the surface characteristics of the SiO_2 substrate and are further supported by X-ray photoemission spectra (Figure 3b). We clearly observe that the p-doping-induced blue shift (lower binding energy) of graphene C_{1s} peak due to the SiO_2 substrate and the n-doping-induced red shift (higher binding energy) of the peak due to the NH_2−SAM-modified SiO_2 substrate.[22]

To examine the electrical performance of graphene films on SAM-modified SiO_2 substrates, we fabricated graphene field-effect transistors (FETs) with Au source/drain electrodes. A schematic of the graphene FETs having SAMs as an insertion layer between the graphene and SiO_2 dielectric is shown in Figure 3c. Figure 3d shows the representative transfer characteristics of graphene FETs of 10−15 devices on the NH_2− and CH_3−SAM-modified SiO_2 as well as the untreated SiO_2 dielectric. The Dirac point, where electron and hole conduction meet (or type of majority carriers change), drastically changes

Table 1. Electrical Properties of the Graphene FETs on Different SAM-Modified SiO_2/Si Substrates (Average Values of 10−15 Devices)[a]

	CH_3	NH_2	SiO_2
Dirac voltage (V)	10 (±1)	−110 (±10)	43 (±5)
hole mobility (10^3 cm^2/(V s))	2.7 (±0.1)	1.8 (±0.2)	1.6 (±0.2)
electron mobility (10^3 cm^2/(V s))	1.5 (±0.1)	0.7 (±0.1)	0.5 (±0.2)

[a] CH_3: octadecyltrichlorosilane; NH_2: aminotriethoxysilane; SiO_2: untreated.

according to the surface characteristics of the dielectric. In untreated SiO_2, the Dirac point voltage is +43 V, which is illustrated by p-doping of graphene, as previously discussed. The Dirac point voltage is −110 V for NH_2−SAMs. This huge shift of Dirac point to negative voltage is explained by n-doping of graphene by the NH_2 functional groups in SAMs. For the CH_3−SAMs, the Dirac point shifts to a slightly positive value (+10 V), which explains that the effect of doping is relatively small.

The hole and electron mobility of each device was calculated in the linear regime using the equation

$$I_D = \frac{WC_i}{L} V_D \mu (V_G - V_T) \qquad (2)$$

where $C_i = 1.08 \times 10^{-8}$ F cm^{-2}, $V_D = 0.1$ V, $W = 1000$ μm, and $L = 30$ μm.

The calculated average hole and electron mobilities (10−15 devices) depending on surface characteristics of the SiO_2 dielectric are shown in Table 1. For the CH_3−SAMs, hole and electron mobilities are 2700 and 1500 cm^2/(V s), respectively. Mobilities drop abruptly when graphene is doped by SiO_2 (p-doping) or NH_2−SAMs (n-doping). Because doping is known to increase charged impurities, the field-effect mobility decreases by scattering from these impurities.[23,24] For this reason, hole and electron mobilties show the highest values for the CH_3−SAM-modified SiO_2, where doping is significantly suppressed by the CH_3−SAM functional groups on SiO_2. This result is consistent with the recent study by Lafkioti et al., which reports the increase in field-effect mobility in HMDS-treated SiO_2, where the doping is significantly reduced by the hydrophobic nature of HMDS.[25]

Excess charge carriers induced by doping can be calculated by utilizing the equation[3]

$$n = \eta |V_n| \qquad (3)$$

where $\eta = 7.2 \times 10^{10}$ cm^{-2} V^{-1} and V_n is the Dirac point voltage. The excess charge carrier density of graphene on the NH_2−SAM-modified SiO_2 and the untreated SiO_2 are 7.9×10^{12} (electron) and 3.1×10^{12} (hole) cm^{-2}, respectively. These densities of excess charge carriers are related to the energy position of the Dirac point by the equation.[26]

$$E_D = \hbar v_F \sqrt{\pi n} \qquad (4)$$

where $v_F = 1.1 \times 10^6$ ms^{-1} in the literature and n = charge carrier density. The calculated energy position of the Dirac point is 0.36 eV for the NH_2−SAM-modified SiO_2 and 0.23 eV for the untreated SiO_2. These values correlate well with the shift of the graphene work function from the reference CH_3−SAM-modified SiO_2 (Figure 3a).
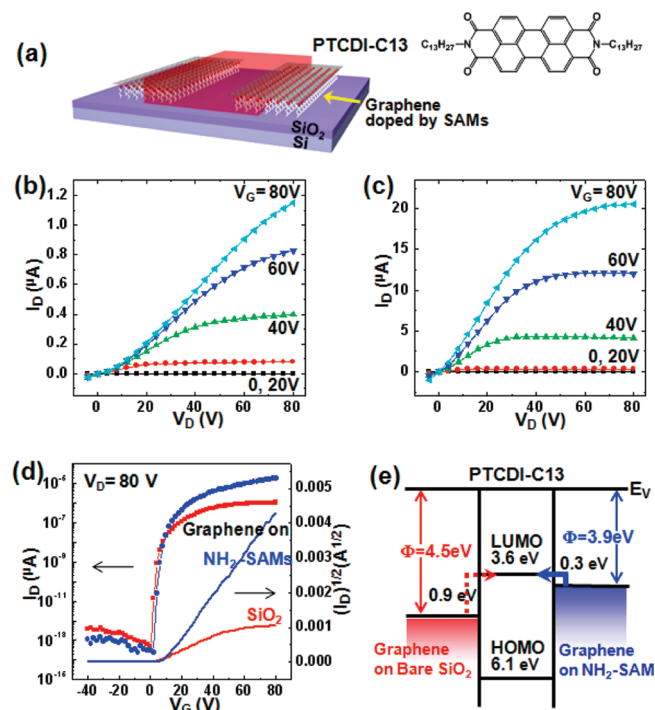
Figure 4. (a) Chemical structure of *N,N'*-ditridecyl-3,4,9,10-perylene-tetracarboxylic diimide (PTCDI-C13) and schematic FET structure using PTCDI-13 as active layer and graphene as source/drain (S/D) electrodes. (b) Output characteristics of n-type PTCDI-C13 FETs with graphene S/D electrodes on untreated SiO_2. (c) Output characteristics of PTCDI-C13 FET with graphene S/D electrodes on NH_2–SAMs. (d) Transfer characteristics of PTCDI-C13 FETs with graphene S/D electrodes on different SAM-modified SiO_2. (e) Schematic band diagrams of PTCDI-C13 and graphene on different SAMs. Energy levels of PTCDI-13 are taken from the literature.[27] V_D: drain voltage; V_G: gate voltage; I_D: drain current.

Because the work function of graphene is easily controlled by SAMs, this information can be utilized to enhance the electrical performance of organic electronic devices using graphene electrodes. To examine work-function-dependent electrical properties of n-type *N,N'*-ditridecyl-3,4,9,10-perylenetetracarboxylic diimide (PTCDI-C13) thin-films, we fabricated bottom-contact organic field-effect transistors (OFETs) with graphene source/drain (S/D) electrodes doped by either NH_2–SAM-modified SiO_2 or untreated SiO_2. (See Figure 4a for chemical structure of PTCDI-13 and device structure.) The detailed fabrication steps of PTCDI-C13 FETs are shown schematically in Figure S2 of the Supporting Information. In this process, the patterned graphene S/D electrodes were selectively doped by NH_2–SAMs or SiO_2, whereas the active channel between dielectric and semiconductor remained the same. Therefore, it can be said that variation in device performances is attributed solely to the work function of graphene-modulated SAMs. Figure 4b,c show the output characteristics of PTCDI-C13 FETs that utilize graphene S/D electrodes with different doping levels (or work functions). In addition to the increased saturation current, the S-shaped non-Ohmic behavior at low V_D is largely reduced when the substrate in contact with graphene changes from SiO_2 to NH_2–SAMs. This observed non-Ohmic behavior can be found in S/D electrodes with mismatched work function where the injection barrier from electrode to channel is large.[19] Detailed device

performances were obtained by analyzing transfer characteristics (Figure 4d). Average field effect mobilities obtained from 10 to 15 devices were 0.11 ± 0.05 $cm^2/(V\ s)$ for NH_2–SAM-modified-SiO_2 and 0.01 ± 0.01 $cm^2/(V\ s)$ for untreated SiO_2. The enhanced field-effect mobility can be explained by different injection capabilities rather than changes to the mobility of the PTCDI-13 channel, which is nominally identical for the two device types. This is also consistent with the reduction of S-shaped I_D–V_D curves for the device with NH_2–SAMs treatment. The work function of graphene is lowered to 3.9 eV for NH_2–SAM-modified SiO_2, so electron injection is facilitated at this low work function graphene electrode (Figure 4e). Graphene on SiO_2 has a higher work function of 4.5 eV, which leads to a high injection barrier (0.9 eV) and correspondingly low field-effect mobility in n-type PTCDI-C13 FETs.

In conclusion, we have described a method to optimize the performance of graphene-based OFETs utilizing the work-function engineering by functionalizing the substrate with SAMs, showing ~10 times enhancements in the charge carrier mobility and the on–off ratio of OFETs. The doping type, carrier concentration, and Fermi energy level from the Dirac point are tuned by the surface characteristics of SAMs inserted between graphene and silicon oxide substrate, which were confirmed by XPS, UPS, Raman spectroscopy, and graphene FETs. Considering the patternability and robustness of SAMs, the present method would find numerous applications in graphene-based organic electronics and optoelectronic devices such as organic light-emitting diodes and organic photovoltaic devices.

■ ASSOCIATED CONTENT

ⓢ Supporting Information. Detailed fabrication procedure of SAMs with their characteristics. This material is available free of charge via the Internet at http://pubs.acs.org.

■ AUTHOR INFORMATION

Corresponding Author
*E-mail: kim@postech.ac.kr (K.S.K.), kwcho@postech.ac.kr (K.C.), and byunghee@skku.edu (B.H.H.).

Author Contributions
[⊥]J. Park and W. H. Lee contributed equally to this work.

■ ACKNOWLEDGMENT

■ REFERENCES

(1) Gierz, I.; Riedl, C.; Starke, U.; Ast, C. R.; Kern, K. Atomic Hole Doping of Graphene. *Nano Lett.* **2008**, *8*, 4603–4607.

(2) Schedin, F.; Geim, A. K.; Morozov, S. V.; Hill, E. W.; Blake, P.; Katsnelson, M. I.; Novoselov, K. S. Detection of Individual Gas Molecules Adsorbed on Graphene. *Nat. Mater.* **2007**, *6*, 652–655.

(3) Pisana, S.; Lazzeri, M.; Casiraghi, C.; Novoselov, K. S.; Geim, A. K.; Ferrari, A. C.; Mauri, F. Breakdown of the Adiabatic

844

dx.doi.org/10.1021/jz200265w |*J. Phys. Chem. Lett.* 2011, 2, 841–845

Born-Oppenheimer Approximation in Graphene. *Nat. Mater.* **2007**, *6*, 198–201.

(4) Das, A.; Pisana, S.; Chakraborty, B.; Piscanec, S.; Saha, S. K.; Waghmare, U. V.; Novoselov, K. S.; Krishnamurthy, H. R.; Geim, A. K.; Ferrari, A. C.; et al. Monitoring Dopants by Raman Scattering in an Electrochemically Top-Gated Graphene Transistor. *Nat. Nanotechnol.* **2008**, *3*, 210–215.

(5) Farmer, D. B.; Golizadeh-Mojarad, R.; Perebeinos, V.; Lin, Y. M.; Tulevski, G. S.; Tsang, J. C.; Avouris, P. Chemical Doping and Electron-Hole Conduction Asymmetry in Graphene Devices. *Nano Lett.* **2009**, *9*, 388–392.

(6) Rao, C. N. R.; Sood, A. K.; Voggu, R.; Subrahmanyam, K. S. Some Novel Attributes of Graphene. *J. Phys. Chem. Lett.* **2010**, *1*, 572.

(7) Giovannetti, G.; Khomyakov, P. A.; Brocks, G.; Karpan, V. M.; van den Brink, J.; Kelly, P. J. Doping Graphene with Metal Contacts. *Phys. Rev. Lett.* **2008**, *101*, 026803.

(8) Chen, W.; Chen, S.; Qi, D. C.; Gao, X. Y.; Wee, A. T. S. Surface Transfer p-Type Doping of Epitaxial Graphene. *J. Am. Chem. Soc.* **2007**, *129*, 10418–10422.

(9) Lohmann, T.; von Klitzing, K.; Smet, J. H. Four-Terminal Magneto-Transport in Graphene p-n Junctions Created by Spatially Selective Doping. *Nano Lett.* **2009**, *9*, 1973–1979.

(10) DiBenedetto, S. A.; Facchetti, A.; Ratner, M. A.; Marks, T. J. Molecular Self-Assembled Monolayers and Multilayers for Organic and Unconventional Inorganic Thin-Film Transistor Applications. *Adv. Mater.* **2009**, *21*, 1407–1433.

(11) Ulman, A. Formation and structure of self-assembled Monolayers. *Chem. Rev.* **1996**, *96*, 1533–1554.

(12) Lee, W. H.; Cho, J. H.; Cho, K. Control of Mesoscale and Nanoscale Ordering of Organic Semiconductors at the Gate Dielectric/Semiconductor Interface for Organic Transistors. *J. Mater. Chem.* **2010**, *20*, 2549–2561.

(13) Li, X. S.; Cai, W. W.; An, J. H.; Kim, S.; Nah, J.; Yang, D. X.; Piner, R.; Velamakanni, A.; Jung, I.; Tutuc, E.; et al. Large-Area Synthesis of High-Quality and Uniform Graphene Films on Copper Foils. *Science* **2009**, *324*, 1312–1314.

(14) Bae, S.; Kim, H.; Lee, Y.; Xu, X. F.; Park, J. S.; Zheng, Y.; Balakrishnan, J.; Lei, T.; Kim, H. R.; Song, Y. I.; et al. Roll-to-Roll Production of 30-in. Graphene Films for Transparent Electrodes. *Nat. Nanotechnol.* **2010**, *5*, 574–578.

(15) Kim, K. S.; Zhao, Y.; Jang, H.; Lee, S. Y.; Kim, J. M.; Kim, K. S.; Ahn, J. H.; Kim, P.; Choi, J. Y.; Hong, B. H. Large-Scale Pattern Growth of Graphene Films for Stretchable Transparent Electrodes. *Nature* **2009**, *457*, 706–710.

(16) Jang, Y.; Cho, J. H.; Kim, D. H.; Park, Y. D.; Hwang, M.; Cho, K. Effects of the Permanent Dipoles of Self-Assembled Monolayer-Treated Insulator Surfaces on the Field-Effect Mobility of a Pentacene Thin-Film Transistor. *Appl. Phys. Lett.* **2007**, *90*, 132104.

(17) Casiraghi, C. Doping Dependence of the Raman Peaks Intensity of Graphene Close to the Dirac Point. *Phys. Rev. B* **2009**, *80*, 233407.

(18) Wei, D. C.; Liu, Y. Q.; Wang, Y.; Zhang, H. L.; Huang, L. P.; Yu, G. Synthesis of N-Doped Graphene by Chemical Vapor Deposition and Its Electrical Properties. *Nano Lett.* **2009**, *9*, 1752–1758.

(19) Ishii, H.; Sugiyama, K.; Ito, E.; Seki, K. Energy Level Alignment and Interfacial Electronic Structures at Organic Metal and Organic Interfaces. *Adv. Mater.* **1999**, *11*, 605.

(20) Berciaud, S.; Ryu, S.; Brus, L. E.; Heinz, T. F. Probing the Intrinsic Properties of Exfoliated Graphene: Raman Spectroscopy of Free-Standing Monolayers. *Nano Lett.* **2009**, *9*, 346–352.

(21) Nourbakhsh, A.; Cantoro, M.; Klekachev, A.; Clemente, F.; Soree, B.; van der Veen, M. H.; Vosch, T.; Stesmans, A.; Sels, B.; De Gendt, S. Tuning the Fermi Level of SiO₂-Supported Single-Layer Graphene by Thermal Annealing. *J. Phys. Chem. C* **2010**, *114*, 6894–6900.

(22) Geng, H. Z.; Kim, K. K.; So, K. P.; Lee, Y. S.; Chang, Y.; Lee, Y. H. Effect of Acid Treatment on Carbon Nanotube-Based Flexible Transparent Conducting Films. *J. Am. Chem. Soc.* **2007**, *129*, 7758.

(23) Chen, J. H.; Jang, C.; Xiao, S. D.; Ishigami, M.; Fuhrer, M. S. Intrinsic and Extrinsic Performance Limits of Graphene Devices on SiO₂. *Nat Nanotechnol.* **2008**, *3*, 206–209.

(24) Tan, Y. W.; Zhang, Y.; Bolotin, K.; Zhao, Y.; Adam, S.; Hwang, E. H.; Das Sarma, S.; Stormer, H. L.; Kim, P. Measurement of Scattering Rate and Minimum Conductivity in Graphene. *Phys. Rev. Lett.* **2007**, *99*, 246803.

(25) Lafkioti, M.; Krauss, B.; Lohmann, T.; Zschieschang, U.; Klauk, H.; von Klitzing, K.; Smet, J. H. Graphene on a Hydrophobic Substrate: Doping Reduction and Hysteresis Suppression under Ambient Conditions. *Nano Lett.* **2010**, *10*, 1149–1153.

(26) Zhang, Y. B.; Brar, V. W.; Wang, F.; Girit, C.; Yayon, Y.; Panlasigui, M.; Zettl, A.; Crommie, M. F. Giant Phonon-Induced Conductance in Scanning Tunnelling Spectroscopy of Gate-Tunable Graphene. *Nat Phys.* **2008**, *4*, 627–630.

(27) Wan, A. S.; Long, J. P.; Kushto, G.; Makinen, A. J. The Interfacial Chemistry and Energy Level Structure of a Liquid Crystalline Perylene Derivative on Au(111) and Graphite Surfaces. *Chem. Phys. Lett.* **2008**, *463*, 72–77.